ACS Partner Journal
PRECISION CHEMISTRY
pubs.acs.org/PrecisionChem
Article

3D Printed Microfluidic Devices for Integrated Immunoaffinity Extraction, Solid-Phase Extraction, and Fluorescent Labeling of Preterm Birth Biomarkers

Published as part of Precision Chemistry special issue "Precision Diagnostics".

James D. Holladay, Zachary A. Berkheimer, Michael K. Haggard, Jacob B. Nielsen, Gregory P. Nordin, and Adam T. Woolley*

Cite This: *Precis. Chem.* 2025, 3, 261−271

Read Online

ACCESS | Metrics & More | Article Recommendations | Supporting Information

ABSTRACT: A miniaturized, biomarker-based diagnostic for preterm birth (PTB) risk will require multiple sample preparation steps to be integrated in a single platform. To this end, we created a 3D printed microfluidic device that combines immunoaffinity extraction (IAE), solid-phase extraction (SPE), and fluorescent labeling. This device uses an antibody-functionalized IAE monolith to selectively extract PTB biomarkers, a lauryl methacrylate reverse-phase SPE monolith to concentrate and facilitate fluorescent labeling of PTB biomarkers, and 3D printed valves to control flow through the monoliths. The advantageous iterative design process for arriving at a functional device is documented. The IAE/SPE device performed selective, reproducible extractions of three PTB biomarkers from buffer and depleted maternal blood serum, demonstrating its utility for single-biomarker and multiplexed extractions. After tandem extraction and fluorescent labeling, biomarkers eluted from the SPE monolith in a concentrated plug, facilitating future integration with downstream analysis techniques including microchip electrophoresis. This device effectively combines and automates orthogonal chromatographic extraction methods and constitutes a substantial step toward a complete microfluidic PTB prediction platform.

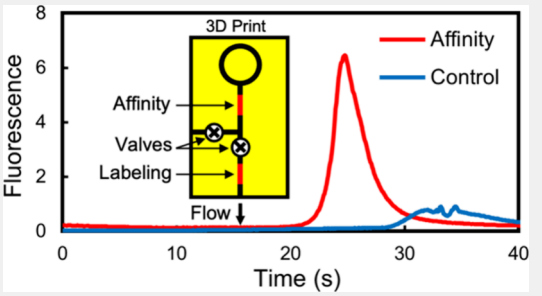

KEYWORDS: *3D printing, lab-on-a-chip, microfluidics, molecular diagnostics, monoliths, point-of-care diagnostics*

INTRODUCTION

Preterm birth (PTB), defined as labor starting earlier than the 37th week of pregnancy, accounts for approximately one million deaths per year.[1] A variety of interventions exist to reduce PTB mortality by delaying labor (progesterone, magnesium sulfate) or accelerating fetal development (corticosteroids), but these interventions require sufficient notice prior to PTB to be fully effective.[2,3] To this end, a variety of clinically useful PTB predictors have been identified. Physiological characteristics, including decreased cervical length, cervical angle, and vaginal pH, are easier to measure, but offer lower selectivity and specificity in PTB diagnosis[4,5] than protein biomarkers in blood serum,[6,7] cervicovaginal fluid,[8] or amniotic fluid.[9] Point-of-care lateral-flow immunoassays detecting cervicovaginal or urinary fetal fibronectin have been approved for use in the European Union; these assays are cheap, provide rapid results, and offer PTB prediction windows of about 1 week.[8,10] Mass spectrometric measurements of multiplexed blood serum biomarkers offer wider prediction windows[11] in exchange for higher costs, more complex sample preparation, and longer time requirements than their immunoassay counterparts.[12] Thus, a solution combining the convenience of a point-of-care test with the wider prediction windows possible from multiplexed serum biomarkers could better address the PTB prediction problem.

During the past 30 years, microfluidic devices have become valuable in a diverse range of fields. Their low sample size requirements and quick analysis times make them cost-effective for processes including organ-on-a-chip studies,[13,14] cell culture,[15,16] polymerase chain reaction,[17,18] and point-of-care diagnostics.[19] Microfluidic devices are particularly important for lab-on-a-chip platforms, where processes normally carried out by multiple, larger instruments are combined and miniaturized within a single device. Traditional fabrication methods, like hot-embossing and soft lithography, limit the complexity of lab-on-a-chip platforms by constraining device features largely to a 2D plane.[20] The development of 3D printing as a microfluidic device fabrication technique permits

Received: November 19, 2024
Revised: February 7, 2025
Accepted: February 10, 2025
Published: March 3, 2025

https://doi.org/10.1021/prechem.4c00092
Precis. Chem. 2025, 3, 261−271

3D features[21] like integrated pumps, valves, and vertical channels to be incorporated within lab-on-a-chip devices, allowing for the miniaturization of more powerful and complex processes.[22] Examples include 3D printed microfluidic serial diluters,[23] optical traps,[24] and concentration gradient generators.[25,26]

A key function of many microfluidic devices is to purify and concentrate biomarkers. Various strategies are used, such as microbeads,[27] membranes,[28] porous polymer monoliths,[29,30] micropillars,[31] or other microstructures. Porous polymer monoliths are particularly useful in microfluidic systems because they can be fabricated *in situ*, possess a high surface-area to volume ratio, and can be morphologically tuned to suit diverse applications.[29] Broadly speaking, monoliths have two primary applications for biomolecule analysis. They can use attached affinity binding agents like antibodies, single-stranded DNA, metal ions, or lectins to perform highly specific extractions.[29] Recent examples of analytes captured using high-specificity monoliths include extracellular vesicles,[32] chikungunya viral RNA,[33] tuberculin,[34] preterm birth biomarkers,[30] and ochratoxin A.[35] Monoliths can also utilize general properties such as hydrophobicity or ionic interactions to preconcentrate classes of biomolecules for further analysis, like proteins,[36,37] glycoproteins,[38] and nucleic acids.[31,39,40] Microfluidic systems that use monoliths generally employ either a high-specificity monolith or a low-specificity one. A system containing orthogonal affinity and general property monoliths would allow for multiple on-chip sample preparation and preconcentration steps, facilitating the analysis of low-concentration biomarkers in complex sample matrices.

Here, we report the development of a 3D printed microfluidic device that integrates immunoaffinity extraction (IAE)[30,41] with solid-phase extraction (SPE)[36] and on-chip fluorescent labeling[42,43] to selectively purify, concentrate, and label PTB biomarkers. The device utilizes an antibody-modified IAE monolith in series with a reverse-phase lauryl methacrylate SPE monolith. Flow within the device is directed by pneumatically controlled 3D printed valves. Tests of the IAE/SPE device using three PTB blood serum biomarkers—corticotropin releasing factor (CRF), ferritin, and lactoferrin—demonstrate extraction and labeling of biomarkers from depleted blood serum samples. This work constitutes a substantial step forward in combining multiple extraction functions in a single miniaturized device, and in providing an integrated microfluidic platform for PTB risk analysis. To our knowledge, it is the first demonstration of the creation and use of orthogonal IAE and SPE monoliths in a microfluidic device.

MATERIALS AND METHODS

Trizma hydrochloride, 4-(2-hydroxyethyl)-1-piperazineethanesulfonic acid (HEPES), acetonitrile (ACN), dodecanol, lauryl methacrylate (LMA), inhibitor removers, polyethylene glycol diacrylate (PEGDA, 258 Da), phenylbis (2,4,6-trimethylbenzoyl)-phosphine oxide (Irgacure 819) and isopropyl alcohol (IPA) were purchased from Sigma-Aldrich (St. Louis, MO). Ethylene dimethacrylate (EDMA), glycidyl methacrylate (GMA), 2,2-dimethoxy-2-phenylacetophenone (DMPA), Amicon ultra centrifugal filters (50 and 3 kDa cutoff), and Alexa Fluor 532 carboxylic acid succinimidyl ester were purchased from ThermoFisher (Waltham, MA). Tris base was purchased from Fisher Scientific (Fair Lawn, NJ). Sodium carbonate, monobasic sodium phosphate, and boric acid were purchased from EMD Millipore (Billerica, MA). Sodium hydroxide pellets were obtained from Mallinckrodt (St. Louis, MO). Cyclohexanol was purchased from Spectrum (New Brunswick, NJ). 2-nitrodiphenylsulfide (NPS) was purchased from TCI America (Portland, OR). UV curing epoxy was purchased from DecorRom (Longgang, Shenzhen). PTFE tubing (#24) was purchased from Zeus (Orangeburg, SC). Solutions were made using 18.3 MΩ cm deionized water filtered by a Barnstead EASY-pure UV/UF system (Dubuque, IA).

CRF was purchased from GenScript (Piscataway, NJ). Ferritin was purchased from EMD Millipore. Lactoferrin was from Sigma-Aldrich. Anti-CRF monoclonal antibodies were obtained from Abnova (Taipei, Taiwan). Antiferritin monoclonal antibodies, antilactoferrin monoclonal antibodies, and High Select Top 14 Depletion midi spin columns were purchased from ThermoFisher. Deidentified, non-PTB maternal blood serum was obtained from Intermountain Healthcare under BYU IRB # IRB2020−133.

PTB Biomarkers

To show the functionality and versatility of the integrated IAE/SPE device, we performed tests using three PTB biomarkers: CRF, ferritin, and lactoferrin. CRF is a 4.8 kDa peptide hormone that is retained less strongly by IAE and SPE monoliths. Ferritin is a 474 kDa protein that is retained tightly by both IAE and SPE monoliths. Lactoferrin is an 80 kDa protein that is also retained strongly on IAE and SPE monoliths, and adheres nonspecifically to surfaces. We chose these biomarkers to ensure our experimental conditions were robust enough to elute tightly bound biomarkers and remove nonspecifically retained analytes while preserving loosely bound biomarkers during rinse steps. These biomarkers were selected from a panel of nine, which together offer a sensitivity of 87% and specificity of 81% 4 weeks prior to PTB.[6] Ideally, an integrated PTB prediction platform would analyze all nine biomarkers; here, these three were selected to cover a range of sizes and analyte complexities.

For experiments involving prelabeled biomarkers, labeling occurred as follows: Biomarkers were dissolved in 100 μL of 10 mM bicarbonate buffer (BCB), pH 10. Alexa Fluor 532 (20 mM) was added to each biomarker and incubated overnight with shaking. Ferritin was labeled using a 30:1 dye:biomarker molar ratio, lactoferrin with 15:1, and CRF with 3:2. The ratios were chosen based on the number of active amine sites per biomarker. Following incubation, the mixtures were transferred to a centrifugal molecular weight cutoff filter. Ferritin and lactoferrin were placed in 50 kDa filters, while CRF was placed in a 3 kDa filter. The filters were filled with 20 mM phosphate, pH 8, then centrifuged for 15 min at 16,000 g to remove excess dye. The phosphate buffer rinses were repeated three more times, and the remaining solutions were diluted to 1 μM in 20 mM phosphate, pH 8. Biomarkers were subsequently diluted to working concentrations in 20 mM phosphate, pH 8. Blood serum was depleted according to the manufacturer's protocol: 100 μL of blood serum was added to a depletion column, which was then incubated at room temperature for 10 min with gentle shaking. The column was placed in a 15 mL falcon tube and centrifuged at 1000 g for 2 min. Approximately 1.5 mL of buffer-diluted depleted serum was obtained from this process; this depleted serum was stored at −20 °C until use.

3D Printing

We carried out 3D printing as in prior publications.[44] Briefly, we used OpenSCAD (www.openscad.org) to design the 3D printed devices. After conversion of the 3D models to STL files, they were sliced along the *z*-axis into 10 μm layers. 3D printed devices were made using a custom digital light processing stereolithography 3D printer with a custom resin consisting of PEGDA, NPS, and Irgacure 819, as described previously.[44]

Monolith Preparation

IAE and SPE monoliths were prepared using procedures modified from Parker et al.[41] and Bickham et al.,[36] respectively. IAE monoliths were composed of 27% GMA monomer and 13% EDMA cross-linker, with 51% dodecanol and 9% cyclohexanol as porogens, and 1% DMPA photoinitiator. SPE monoliths were composed of 15% LMA monomer, 20% EDMA cross-linker, and 65% dodecanol porogen, with 1% DMPA photoinitiator. To ensure homogeneity, the monolith mixtures were sonicated for 10 min prior to use. For 5-monolith devices (Figure S1),[36] either the IAE or SPE mixture was loaded into

https://doi.org/10.1021/prechem.4c00092
Precis. Chem. 2025, 3, 261−271

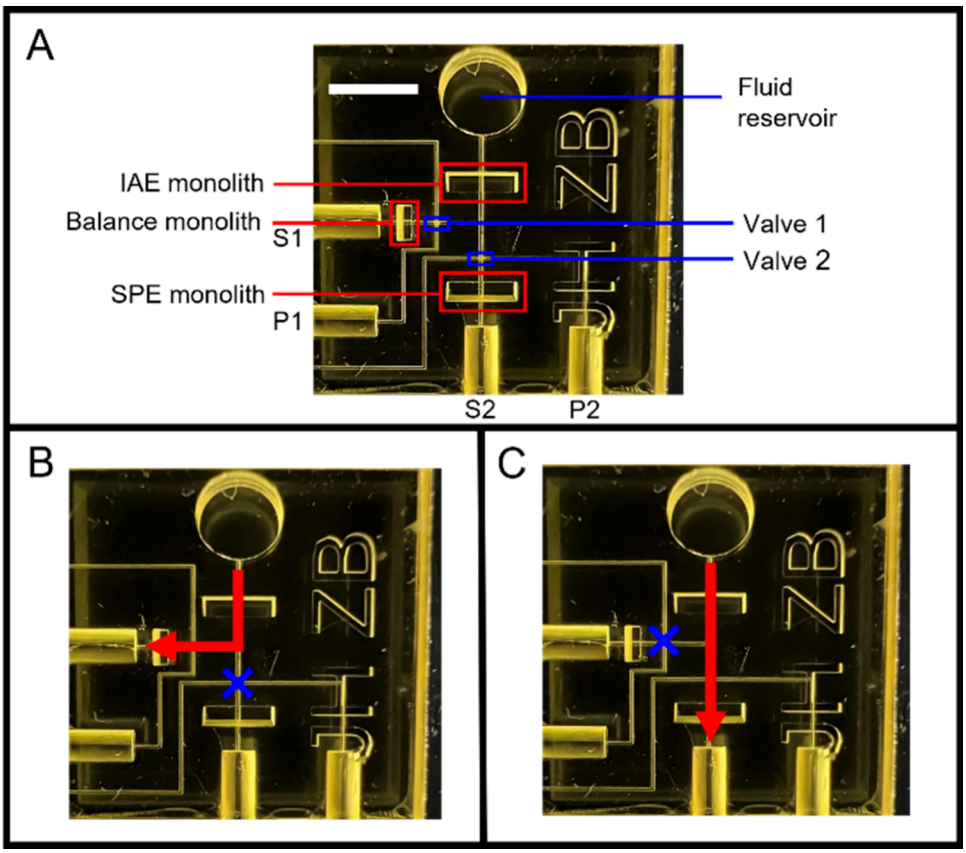

Figure 1. Schematic of integrated IAE/SPE device. (A) Device features. S1, S2: vacuum (suction) ports 1 and 2. P1, P2: pneumatic ports 1 and 2. Scale bar is 3 mm. (B) Device set to direct flow through the IAE and balance monoliths. Pressure is applied to P2, closing valve 2. Vacuum applied through S1. (C) Directing flow through IAE and SPE monoliths. Valve 1 is closed by pressure through P1, vacuum applied through S2.

the microfluidic channels via capillary action. The devices were masked with electrical tape, leaving only the polymerization window exposed, and polymerized under a UV lamp for either 7.5 min (IAE) or 8.5 min (SPE). Following polymerization, the monoliths were rinsed with IPA for 30 min, then for 10 min with 20 mM borate pH 8. To functionalize IAE monoliths, 1 mg/mL antibody was flowed through the monolith for 1 min. The reservoirs were then filled with 20 mM borate pH 8, and the devices were incubated overnight at room temperature in a sealed humid container to allow primary amines on the antibodies to covalently attach to GMA in the polymer. The next day, the monoliths were incubated in 20 mM Tris, pH 8, for 2 h to block any remaining reactive sites. For control devices, antibodies were omitted and the monoliths were incubated in Tris overnight.

For integrated IAE/SPE devices, a similar procedure was followed, except the SPE and balance monoliths were polymerized first, followed by a 30 min IPA rinse and a 10 min rinse with IAE monolith mixture. The IAE monolith was then polymerized, and the monoliths were rinsed again for 30 min with IPA, then for 10 min with 20 mM borate pH 8. IAE monoliths were functionalized using the procedure described above. After polymerization and functionalization of the monoliths, PTFE tubing was inserted into the vacuum and pneumatic ports and secured using epoxy. During experiments, blunted 25-gauge needles were used to connect the pneumatic ports to a custom-designed pressure system (https://github.com/3D-Printing-for-Microfluidics/valve-control) running at 35 PSI.[45]

Scanning Electron Microscopy (SEM)

SEM images of monoliths were obtained by removing the device from the glass slide using a razor blade, then slicing horizontally across the polymerization window to reveal the monolith. The exposed monoliths were attached to stubs using carbon tape, and sputter coated using 80:20 Au:Pd (Q150T ES Sputterer, Quorum Technologies, Lewes, East Sussex, UK). Images were taken using an Apreo C Low-vacuum SEM (Thermo) in high vacuum mode at 10 kV. Image analysis was performed using ImageJ.

Experimental Setup

Experiments were performed using the laser-induced fluorescence setup described by Parker et al.[41] Fluorescence was induced using a 532 nm laser and detected using a Hamamatsu photomultiplier tube, the signal from which was digitized using custom LabView software. For IAE experiments, channels were filled with 20 mM HEPES pH 8, and vacuum was applied for 1 min for an initial rinse. The reservoir was filled with 5 μL of biomarker solution, then vacuum was reapplied for 1 min to load analyte onto the monolith. The reservoir was emptied and rinsed with 20 mM HEPES pH 8 with 0.1% Tween, then HEPES buffer was drawn through to remove nonspecifically retained biomarker. Rinsing continued until fluorescence returned to baseline, about 1−2 min. To elute, 10 mM NaOH (pH 12) was drawn through the monolith until fluorescence returned to baseline, about 1 min.

For SPE experiments, the monolith was rinsed with 20 mM BCB pH 10 for 3 min before loading biomarker onto the column for 90 s. If unlabeled biomarkers were used, 1 μM Alexa Fluor 532 in 20 mM BCB pH 10 was next flowed through the column for 90 s. Vacuum was removed, and the device was incubated at room temperature with the laser off for 30 min to allow time for more complete labeling. If prelabeled biomarkers were used, the Alexa Fluor flow and incubation steps were omitted. The monoliths were then rinsed twice to remove excess dye, once for 90 s with 20 mM BCB pH 10 and once for 90 s with 30% ACN in 20 mM BCB pH 10. Analyte was eluted by drawing through 90% ACN in 20 mM BCB pH 10 for 90 s.

Integrated IAE/SPE experiments were conducted using the procedures described above, with flow times adjusted for the slower flow rate in the integrated device with two monoliths. The initial rinse, loading and postload rinse steps for the IAE portion were

https://doi.org/10.1021/prechem.4c00092
Precis. Chem. 2025, 3, 261−271

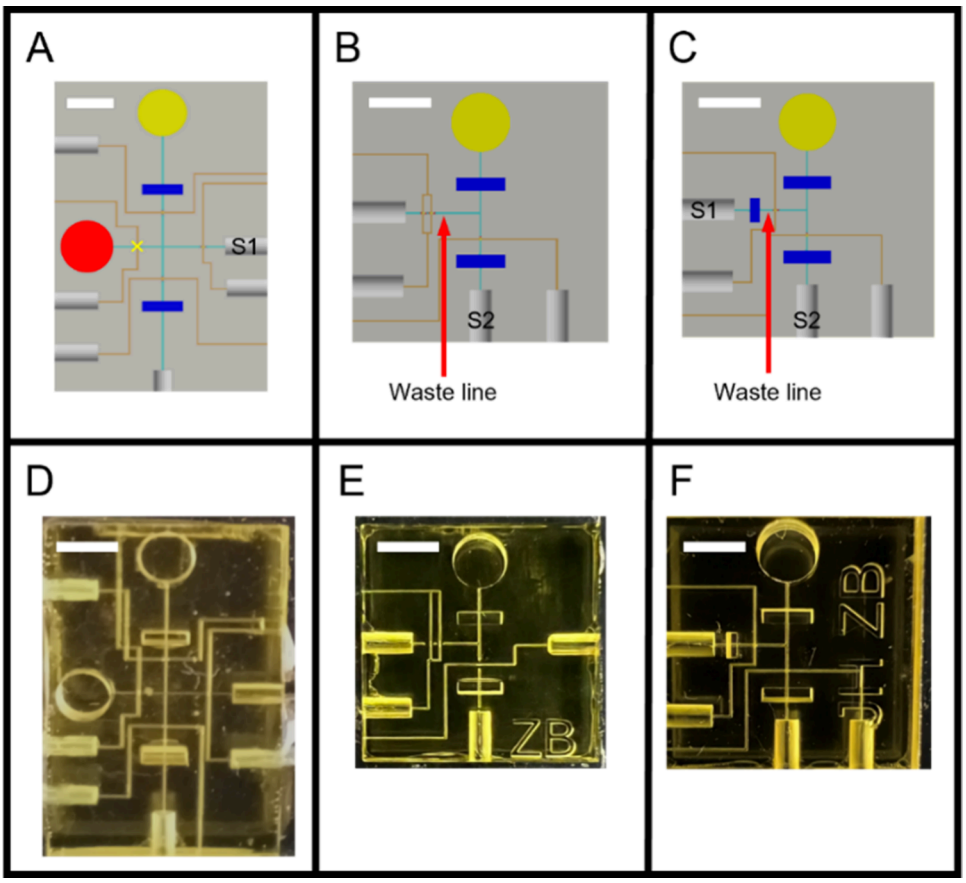

Figure 2. IAE/SPE integrated device design progression. (A−C) Top views of the CAD schematics for a few iterations of the integrated device. (D−F) Photographs of 3D printed devices. (A, D) Initial dual-reservoir, 4-valve design with 50 μm × 50 μm channels. SPE reservoir marked in red, valve 1 marked with a yellow "×". (B, E) Compact, simplified design with 100 μm × 100 μm channels and two valves on the waste line. (C, F) Final design with 100 μm × 100 μm channels and a balance monolith on the waste line. Scale bars are 3 mm.

performed with flow directed through the IAE and balance monoliths and out the waste line (Figure 1A,B). Vacuum was applied to S1, and valve 2 was closed via pressure through P2. The initial rinse and loading steps lasted 2 min each, and the second rinse step took about 2−5 min to reach baseline, depending on the biomarker. IAE elution and subsequent SPE steps occurred with flow through the IAE and SPE monoliths (Figure 1A,C). Vacuum was applied to S2 and valve 1 was closed via pressure through P1. During elution, fluid was drawn through for at least 8 min to ensure full transfer of analyte from the IAE monolith to the SPE monolith. If on-chip labeling was performed, Alexa Fluor was then pulled through for 3 min, followed by a 30 min room temperature incubation. During incubation, flow was temporarily redirected through the IAE and balance monoliths (as during the IAE monolith loading step, Figure 1B), so the monoliths could be rinsed with BCB and 30% ACN for 3 min each, removing any remaining analyte and preventing dye from labeling the antibodies on the IAE monolith. If using prelabeled biomarker, the Alexa Fluor 532, incubation, and BCB/30% ACN IAE monolith rinse steps were skipped. The device was then set so flow once again passed through the IAE and SPE monoliths (Figure 1C), and BCB and 30% ACN were drawn through successively for 3 min each to remove excess dye. Finally, biomarker was eluted from the SPE monolith using 90% ACN for 3 min, with fluorescence detection occurring between the monolith and S2 (Figure 1).

RESULTS AND DISCUSSION

A dual-monolith IAE/SPE design enabled orthogonal mechanisms for biomarker enrichment and facilitated on-chip analyte labeling. Separating the IAE and SPE processes using on-chip valves allowed appropriate eluents to be used with each monolith, while keeping the protein labeling reagents away from the IAE monolith. This minimized fluorescent labeling of analytes nonspecifically retained on the IAE monolith, and prevented the antibodies on the IAE monolith from becoming labeled, allowing device reuse.

The integrated IAE/SPE device layout was modified approximately 20 times before arriving at the final, fully functional, reliable design. This iterative process was facilitated by the unique characteristics of 3D printing, which enabled modifications to the design to be rapidly implemented and tested, often multiple times per week. Three key versions of the device are discussed below, and information on additional layouts is provided in Table S1. The initial design (Figure 2A,D) had 50 μm × 50 μm channels, four valves, and two reservoirs: one for loading sample onto the IAE monolith (top), and the other for SPE solutions (left, red). The SPE reservoir was included so that solutions would bypass the IAE monolith, facilitating flow during SPE steps and preventing the labeling solution and SPE eluent from encountering antibodies or nonspecifically retained analytes on the IAE monolith. During IAE steps, valve 1 was closed with the intention of preventing flow from the SPE reservoir. However, when vacuum was applied to S1 with valve 1 closed, as indicated by the yellow "×" in Figure 2A, the SPE reservoir still emptied, indicating that valve 1 did not fully block flow. To address this issue, the second reservoir was omitted from subsequent designs.

https://doi.org/10.1021/prechem.4c00092
Precis. Chem. 2025, 3, 261−271

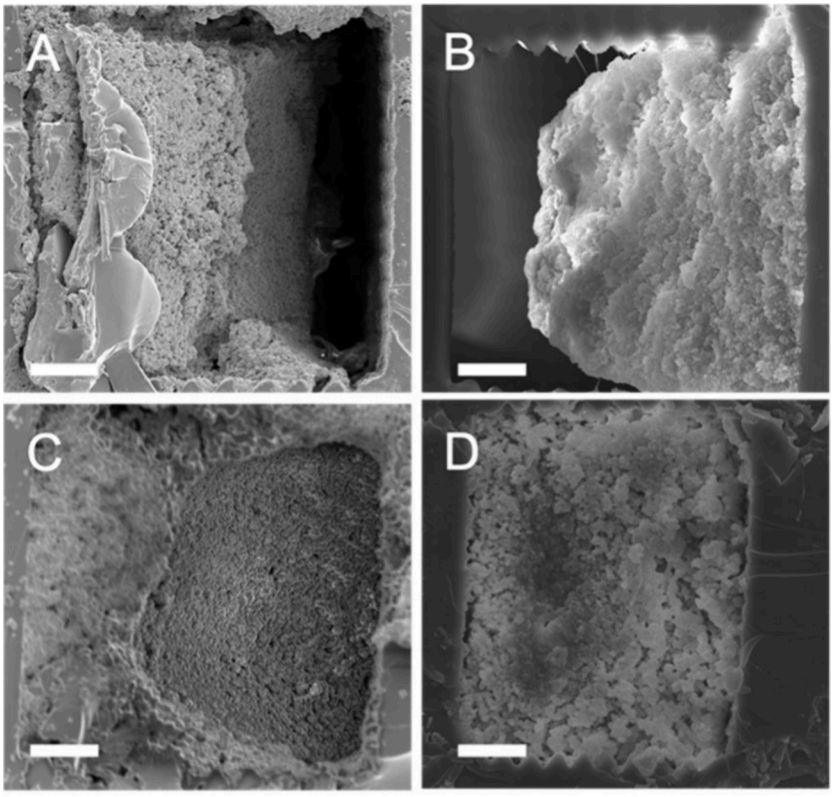

E

Component	Standard	Low porogen
GMA	24%	27%
EDMA	11%	13%
Dodecanol	55%	51%
Cyclohexanol	10%	9%
DMPA	1%	1%

Figure 3. Optimizing monoliths for 100 μm × 100 μm channels. (A-D) SEM micrographs of monoliths polymerized in 100 μm × 100 μm channels taken at 800× magnification, 20 μm scale bars for reference. (A) IAE and (B) SPE monoliths created using formulations optimized for 50 μm × 50 μm channels, leading to incomplete monolith adhesion to channel walls. (C) IAE monolith created using low-porogen monomer mixture. (D) SPE monolith using previous formulation polymerized in a serrated monolith window. (E) Table of IAE monolith compositions. (F) Micrograph of SPE monolith in serrated channel, with 100 μm scale bar for reference. Monoliths were polymerized in a five-monolith test device (Figure S1).

Tests using a valve-free, single-channel, dual-monolith device (Figure S2A) revealed a second issue: vacuum was insufficient to draw flow through two 50 μm × 50 μm monoliths in series. Further testing using a design modified to be operated via syringe pump (Figure S2B) showed that the pressure-driven flow through two monoliths in series often resulted in device delamination between 3D printed layers and subsequent fluid leakage. To reduce backpressure, subsequent designs were created with larger cross-section, 100 μm × 100 μm channels and monoliths. Monolith formulations are cross-section dependent; increasing the cross-sectional area and using the previously reported formulations[30,36] resulted in poor monolith adhesion to the channel walls (Figure 3A,B). Thus, the IAE monoliths were modified by decreasing porogen content by approximately 10% and proportionally increasing monomer and cross-linker content, as noted in Figure 3E. SEM images of these monoliths indicated good adhesion to 100 μm × 100 μm channel walls (Figure 3C), with morphologies similar to IAE monoliths made using the previous formulation.[30] Similar attempts to modify the SPE monoliths did not improve adhesion, but adding periodic serrations to the monolith channel walls through the 3D print design did (Figure 3D,F). We believe the serrations improved adhesion by increasing the surface area of the channel walls. Tests in a device similar to that in Figure S2A, but with 100 μm × 100 μm channels, showed that vacuum was sufficient to draw flow through two serial larger-channel monoliths.

Figures 2B and 2E show the fifteenth iteration of the design. Key changes from the initial layout include elimination of the second reservoir, use of 100 μm × 100 μm channels, addition of serrations to the SPE monolith channel, and a 30% decrease in channel length to further reduce backpressure. Two valves were placed on the waste line with the objective of preventing air from entering the fluid channels when vacuum was applied

https://doi.org/10.1021/prechem.4c00092
Precis. Chem. 2025, 3, 261−271

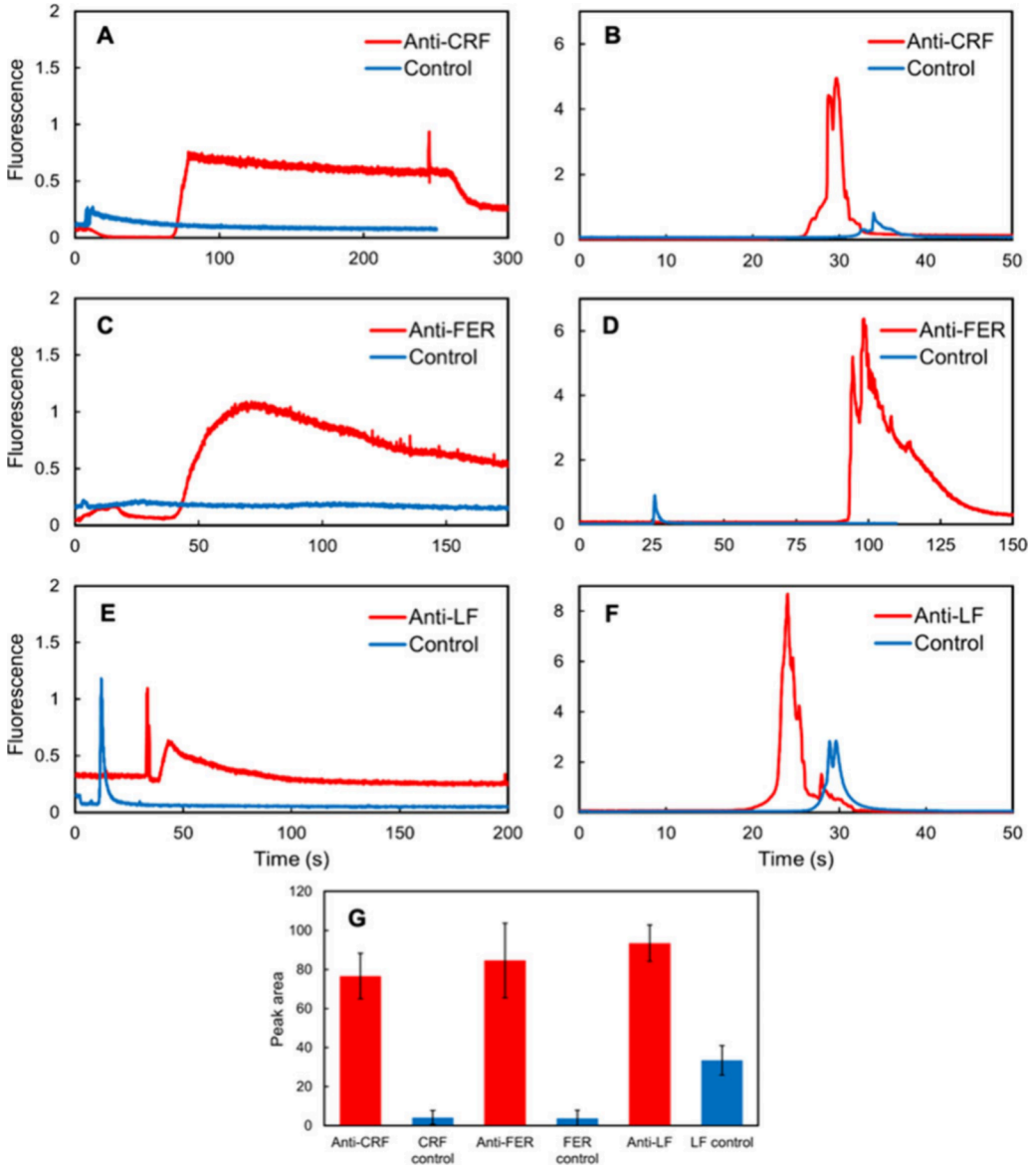

Figure 4. IAE and SPE of prelabeled biomarkers in buffer using the integrated IAE/SPE device. IAE extractions were performed using either an IAE monolith functionalized with antibodies or a Tris-blocked control. (A, C, E) Fluorescence detection of biomarkers eluted from IAE monoliths after extraction from buffer. The eluted biomarkers were recaptured by the SPE monolith. (B, D, F) Fluorescence detection of biomarkers eluted from the SPE monolith. (G) SPE elution peak areas for antibody-functionalized and control devices, measured during the 90% ACN elution step after IAE and SPE. Error bars represent the standard deviation of three replicates. Prelabeled 375 nM CRF, 25 nM ferritin, or 12.5 nM lactoferrin was used for these experiments.

at S2, an issue that had hindered operation of previous versions of the device with just one valve. This approach was partially effective, resulting in select devices that appropriately directed flow, but many still allowed air to pass in from the waste line. For devices containing combinations of channels with monoliths and channels without monoliths, the lower-resistance monolith-free channels offered a more favorable path for flow, even with closed valves. Though a single valve could direct flow through unobstructed channels, two serial valves were still insufficient to fully direct flow through channels containing monoliths.

Figures 2C and 2F show the final, twentieth, design of the integrated IAE/SPE device. It is similar to the one in Figure 2B/F, with rearrangements in the pneumatic channels, elimination of the second valve on the waste line, and the creation of a third monolith near S1. This third monolith, which we called a "balance monolith," is made using the SPE formulation. Its purpose is to restrict flow in the waste line when vacuum is applied to S2, rather than assist in extraction. This balance monolith is separated from the IAE/SPE device functionality by valve 1, and does not incubate with fluorescent label, preventing spuriously retained material from being detected in the experiments. The combination of a closed valve and the balance monolith creates significantly more flow resistance than a monolith alone, directing flow away from the waste line and through channels without closed valves. Moreover, the balance monolith creates a barrier against air entering from the waste line; if air is drawn toward the balance monolith, the surface tension of the remaining liquid in the monolith hinders air from moving in. In operation tests of up to 1 h, no air passed through the balance monolith when valve 1 was closed and vacuum was applied to S2, which is more

https://doi.org/10.1021/prechem.4c00092
Precis. Chem. 2025, 3, 261−271

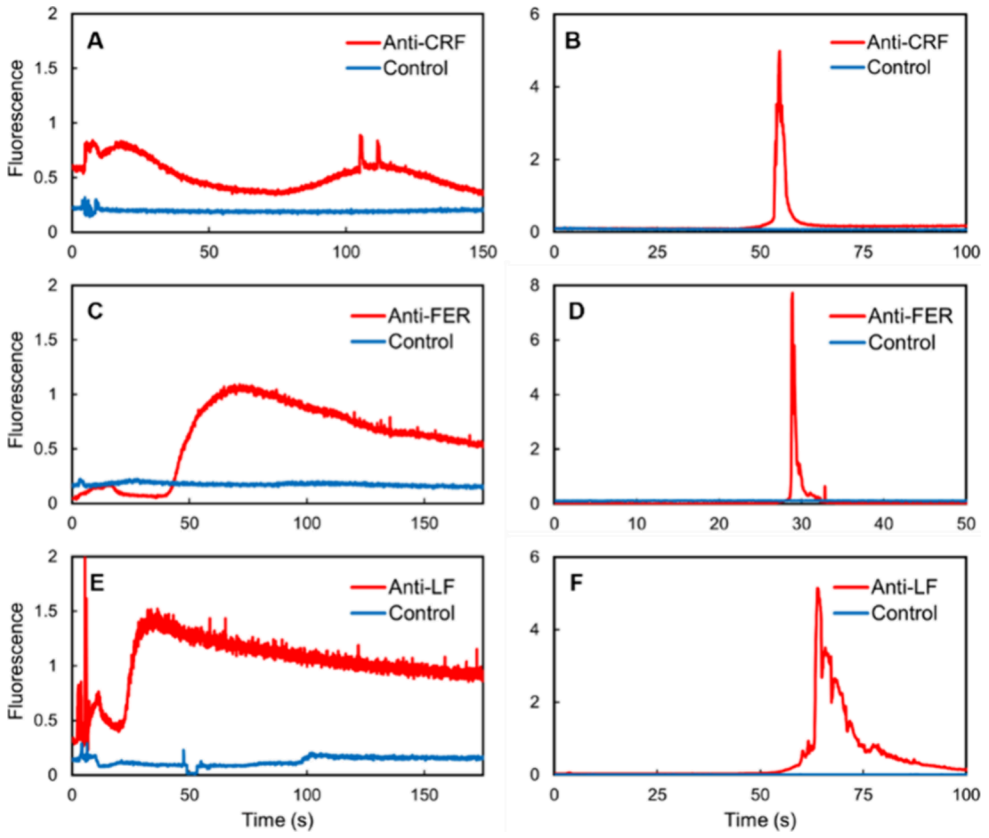

Figure 5. IAE and SPE of prelabeled biomarkers in depleted serum using the integrated IAE/SPE device. IAE extractions were performed using either an IAE monolith functionalized with antibodies or a Tris-blocked control. (A, C, E) Fluorescence detection of biomarkers eluted from IAE monoliths after extraction from depleted serum. The eluted biomarkers were recaptured by the SPE monolith. (B, D, F) Fluorescence detection of biomarkers eluted from the SPE monolith. Prelabeled 375 nM CRF, 25 nM ferritin, or 12.5 nM lactoferrin in depleted blood serum used for these experiments.

than sufficient to prevent air from entering the integrated IAE/SPE device during experiments.

Figure 4 demonstrates integrated IAE/SPE device function using prelabeled biomarkers in buffer. Figures 4A, 4C, and 4E show fluorescence during elution when 10 mM NaOH is flowed through the IAE monolith after retaining prelabeled biomarker. In such experiments and throughout the paper, a "control" device or column is one in which the IAE monolith was not functionalized with antibodies. CRF IAE elution peaks were broad and somewhat variable in shape (Figure 4A). Ferritin generally eluted from the IAE monolith in a broad, but somewhat sharper peak than CRF (Figure 4C). Lactoferrin also eluted in a broad peak, with initial rapidly changing signal (Figure 4E). In all cases, complete IAE elution took about 200−300 s. Little to no elution was observed for CRF and ferritin control columns that lacked the target antibody, indicating that there was minimal nonspecific retention on these IAE monoliths. Lactoferrin control columns showed smaller elution peaks than for IAE columns, indicative of some nonspecific binding inherent to this protein.

In these IAE/SPE devices, the IAE eluate flows through the SPE monolith, which retains analytes through reverse-phase interaction. Figures 4B, 4D, and 4F show fluorescence during elution when 90% ACN is run through the SPE monolith after retention of the IAE eluate and rinsing with BCB and 30% ACN. CRF eluted in a double peak that lasted about 8 s (Figure 4B), ferritin came off in a double peak that lasted about 40 s (Figure 4D), and lactoferrin was removed in a jagged, 12-s single peak (Figure 4F). Elution peaks from SPE monoliths were considerably sharper and taller than those from IAE monoliths, further demonstrating sample enrichment. The formation of a concentrated and temporally narrow sample plug during elution is especially promising for future integration with microchip electrophoresis.[46] Mean and standard deviation values (n = 3) of SPE elution peak areas after retention on anti-CRF, antiferritin, and antilactoferrin functionalized IAE columns are provided in Figure 4G. SPE elution peak areas from anti-CRF and antiferritin devices were approximately 20-fold larger than control peak areas, while those for antilactoferrin devices were 3-fold higher than controls. Based on the control SPE elution peak areas and standard deviations, we estimate the limits of detection under these experimental conditions to be 40 nM, 2 nM, and 5 nM for CRF, ferritin, and lactoferrin, respectively. Clinical serum concentrations for these biomarkers in PTB patients are 0.08 nM, 0.04 nM, and 3 nM for CRF, ferritin, and lactoferrin, respectively,[6] such that further improvements to detection limits are needed, for example through the use of longer and/or higher-capacity monoliths. Improvements to monoliths could also address the somewhat jagged or tailing elution peak characteristics sometimes observed, which may result from low volumes and flow rates used, short lengths of monoliths, dead volumes from valves, and fluorescent labeling efficiency. As one example, the latter could be investigated in future mass spectrometry studies to determine the molecular composition of each band.

https://doi.org/10.1021/prechem.4c00092
Precis. Chem. 2025, 3, 261−271

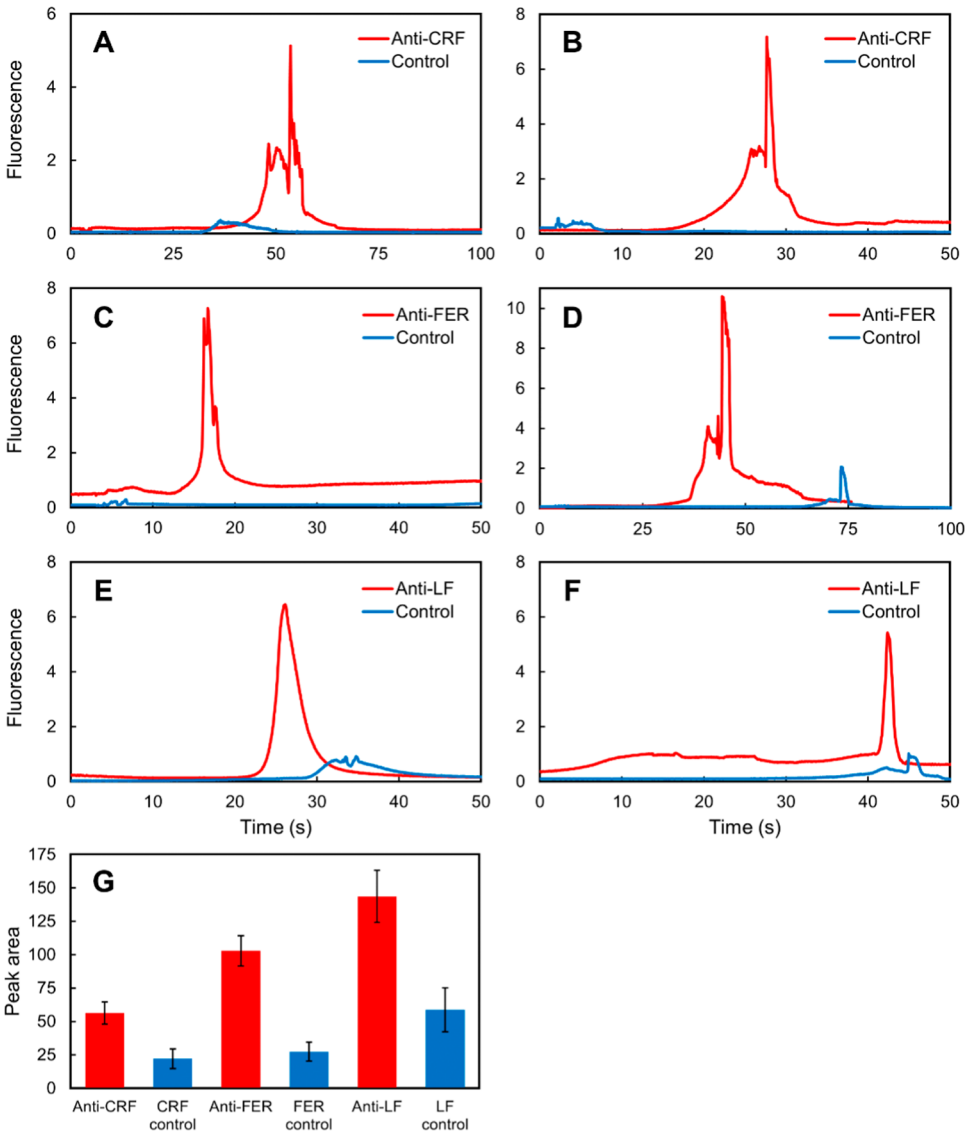

Figure 6. On-column labeling of biomarkers following IAE and SPE. IAE was performed using either an IAE monolith functionalized with antibodies or a Tris-blocked control. (A, C, E) Fluorescence detection of biomarkers eluted from the SPE monolith after IAE extraction from buffer, recapture on SPE monolith, and on-column labeling. (B, D, F) Fluorescence detection of biomarkers eluted from the SPE monolith after IAE extraction from depleted blood serum, recapture on SPE monolith, and on-column labeling. (G) SPE elution peak areas for antibody-functionalized and control devices, measured for extraction from buffer during the 90% ACN elution step after IAE and SPE. Error bars represent the standard deviation of three replicates. Unlabeled 375 nM CRF, 25 nM ferritin, or 12.5 nM lactoferrin used for these experiments.

To evaluate device performance with clinically relevant maternal serum samples, we performed extractions using prelabeled biomarkers spiked into maternal blood serum (Figure 5). Since many abundant proteins such as albumin and immunoglobulins decrease the specificity of immunoaffinity extraction, the serum was depleted of the 14 most abundant proteins prior to use. In contrast to previous work on IAE with depleted serum, which saw broader, taller peaks when extracting from depleted serum compared to buffer,[30] the IAE and SPE elution curves for the integrated IAE/SPE device were relatively unaffected by the change in sample matrix to depleted serum. The greater reproducibility between extracting from buffer and depleted serum could be due to improvements in our IAE rinse buffer,[30] which previously did not include Tween detergent.

Since clinical biomarker analysis involves unlabeled analyte, we also performed experiments retaining unlabeled biomarkers followed by labeling them on-column (Figure 6). PTB biomarkers were extracted from buffer via IAE, eluted, then retained on the SPE monolith. Amine-reactive Alexa Fluor 532 was flowed through the SPE monolith with retained biomarkers and incubated for 30 min to perform fluorescent labeling. Following incubation, the SPE monolith was rinsed to remove excess dye, and then the labeled biomarker was eluted. Figures 6A, 6C, and 6E show the fluorescent signal during SPE elution for biomarkers extracted from buffer and labeled on-column. The peaks for on-column labeled PTB biomarkers exhibited similar sharp, somewhat jagged peak shapes compared to their prelabeled counterparts in Figures 4B, 4D, and 4F. Mean peak areas and standard deviations (n = 3) are provided in Figure 6G. Approximately 25% less CRF was eluted during on-column labeling experiments compared to prelabeled ones. This slight decrease was likely driven by loss of biomarker during the incubation step, since CRF is least

https://doi.org/10.1021/prechem.4c00092
Precis. Chem. 2025, 3, 261−271

strongly retained by SPE monoliths. Compared to experiments with prelabeled biomarker, similar peak areas for ferritin and lactoferrin were eluted for on-column labeling experiments.

The SPE elution peaks for on-column labeled biomarkers extracted from depleted serum (Figures 6B, 6D, and 6F) were similar in size and shape to their buffer solution counterparts. We note that if nonbiomarker serum proteins had also been retained by the IAE monolith, the SPE elution peaks for experiments with depleted serum would have been larger than those for buffer experiments, where there are no off-target proteins present. The similar peak sizes indicate that these IAE monoliths selectively extract the PTB biomarkers of interest, with minimal retention of off-target analytes. Vitally, these experiments also demonstrate the capacity of the IAE/SPE device to selectively extract, purify and label PTB biomarkers from depleted serum, a promising step toward an integrated PTB prediction platform. By integrating a plasma separation component[47−49] and an on-chip depletion column to remove abundant proteins,[50−52] an integrated PTB prediction platform could analyze whole blood samples, eliminating the upstream sample preparation methods utilized herein. Furthermore, analyzing whole blood could improve diagnostic specificity, since clinically relevant proteins may be lost during the serum preparation process.

Since PTB risk assessment is improved by quantifying multiple biomarkers, an IAE/SPE device capable of performing multiplexed extractions is advantageous. Multiplexed experiments were conducted by functionalizing IAE monoliths with equimolar concentrations of anti-CRF, antiferritin, and antilactoferrin antibodies. Device operation followed the procedures described previously, except combinations of prelabeled biomarkers were loaded (CRF only; CRF plus ferritin; or CRF, ferritin, and lactoferrin) and extracted from buffer. Figure 7 shows SPE elution peaks for each of the

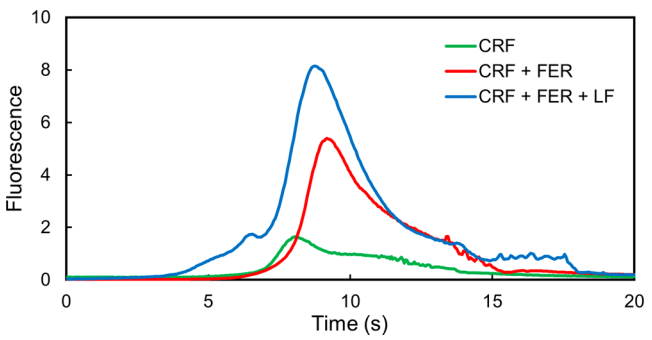

Figure 7. Elution from an SPE monolith following multiplexed IAE extraction. IAE monoliths were functionalized with anti-CRF, antiferritin, and antilactoferrin antibodies. Fluorescence was measured during SPE elution following IAE/SPE of mixtures of biomarkers. Prelabeled 187.5 nM CRF, 12.5 nM ferritin, and 6.3 nM lactoferrin used for these experiments. The initial 50 s of baseline data before each peak were trimmed to allow for clearer comparisons between runs. Tests were performed in random order on a single device.

biomarker combinations. As the number of biomarkers increased from one to three, the peak areas increased, indicating that all three biomarkers were retained on the multiplexed IAE column, eluted and retained on the SPE monolith, and then detected fluorescently during SPE elution. The biomarkers eluted in a single peak, which is beneficial for the formation of sample plugs containing multiple biomarkers during future integration with microchip electrophoresis. Table 1 compares the multiplexed SPE elution peak areas to

Table 1. Comparison of Combined Peak Areas from Single-Biomarker and Multiplexed Experiments

biomarker combination	single antibody[a]	multiplexed[b]
CRF	38 ± 12	41
CRF + FER	81 ± 22	102
CRF + FER + LF	130 ± 24	170

[a]Sum of peak areas as reported in Figure 4G, divided by 2 to account for sample concentration differences between the single-antibody and multiplexed experiments (mean ± standard deviation). [b]Adjusted to correct for photomultiplier tube gain differences between single-antibody and multiplexed experiments.

corresponding sums of peak areas obtained during the single-antibody experiments in Figure 4. Peak areas for the CRF and CRF plus ferritin biomarker combinations were consistent to within one standard deviation, between the multiplexed and single-antibody experiments. The peak area for the multiplexed CRF plus ferritin and lactoferrin combination was larger than the sum of peak areas from single-antibody counterparts. These results demonstrate that for CRF and ferritin, consistency is preserved between single-biomarker and multiplexed experiments. Future experiments should investigate whether the increased lactoferrin retention in multiplexed experiments is the result of interactions between lactoferrin and the other biomarkers, off-target binding, or some other effect.

CONCLUSION

We have reported on a 3D printed integrated IAE/SPE device for purification and on-device labeling of preterm birth biomarkers. Numerous iterations of this device were designed and tested before arriving at its final, functional form, illustrating the utility of 3D printing for convenient layout reconfiguration. Furthermore, key features of the device, including integrated valves and channels arranged in three dimensions, were only possible due to the ability of 3D printing to create nearly arbitrary shapes. We have shown that this integrated IAE/SPE device is capable of selectively extracting analyte from depleted blood serum, enriching it, labeling it, and releasing it in a concentrated plug for downstream analysis. We have further demonstrated the use of these devices for performing multiplexed biomarker extractions. Future integration with a plasma separation component, depletion column, and microchip electrophoresis system[46] will yield a complete platform for point-of-care PTB prediction. Moreover, the fact that the integrated IAE/SPE device functions well with both small peptides and large proteins makes it promising for application to biomarkers for numerous diseases, not just PTB.

ASSOCIATED CONTENT

Supporting Information

The Supporting Information is available free of charge at https://pubs.acs.org/doi/10.1021/prechem.4c00092.

Photographs of monolith test devices and flow test devices and descriptions of CAD files (PDF)
CAD files for selected device designs (ZIP)

https://doi.org/10.1021/prechem.4c00092
Precis. Chem. 2025, 3, 261−271

AUTHOR INFORMATION

Corresponding Author

Adam T. Woolley − *Department of Chemistry and Biochemistry, Brigham Young University, Provo, Utah 84602, United States;* orcid.org/0000-0002-4699-8094; Phone: 1-801-422-1701; Email: atw@byu.edu

Authors

James D. Holladay − *Department of Chemistry and Biochemistry, Brigham Young University, Provo, Utah 84602, United States*

Zachary A. Berkheimer − *Department of Chemistry and Biochemistry, Brigham Young University, Provo, Utah 84602, United States;* Present Address: Department of Biochemistry, University of Utah, Salt Lake City, UT 84112, USA

Michael K. Haggard − *Department of Chemistry and Biochemistry, Brigham Young University, Provo, Utah 84602, United States*

Jacob B. Nielsen − *Department of Chemistry and Biochemistry, Brigham Young University, Provo, Utah 84602, United States;* Present Address: Department of Pathology, Houston Methodist Hospital, Houston, TX 77030, USA.

Gregory P. Nordin − *Department of Electrical and Computer Engineering, Brigham Young University, Provo, Utah 84602, United States;* orcid.org/0000-0001-7241-5764

Complete contact information is available at: https://pubs.acs.org/10.1021/prechem.4c00092

Notes

The authors declare no competing financial interest.

ACKNOWLEDGMENTS

We thank the NIH for funding this work (R01 EB027096 and R15 GM123405), Brigham Young University for undergraduate research awards that supported J.D.H., Z.A.B., and M.K.H., and a Roland K. Robbins Fellowship that supported J.B.N. We also thank Anum Tahir for assistance with sample preparation and Joule Esene for help with 3D printing. Finally, we thank the Brigham Young University Electron Microscopy Facility for access to their equipment for this project.

REFERENCES

(1) Ohuma, E. O.; Moller, A.-B.; Bradley, E.; Chakwera, S.; Hussain-Alkhateeb, L.; Lewin, A.; Okwaraji, Y. B.; Mahanani, W. R.; Johansson, E. W.; Lavin, T.; et al. National, regional, and global estimates of preterm birth in 2020, with trends from 2010: a systematic analysis. *Lancet* **2023**, *402* (10409), 1261−1271.

(2) Patel, S. S.; Ludmir, J. Drugs for the Treatment and Prevention of Preterm Labor. *Clin Perinatol* **2019**, *46* (2), 159−172.

(3) Khandre, V.; Potdar, J.; Keerti, A. Preterm Birth: An Overview. *Cureus* **2022**, *14* (12), No. e33006.

(4) Luechathananon, S.; Songthamwat, M.; Chaiyarach, S. Uterocervical Angle and Cervical Length as a Tool to Predict Preterm Birth in Threatened Preterm Labor. *Int. J. Womens Health* **2021**, *13*, 153−159.

(5) Olarinoye, A. O.; Olaomo, N. O.; Adesina, K. T.; Ezeoke, G. G.; Aboyeji, A. P. Comparative diagnosis of premature rupture of membrane by nitrazine test, urea, and creatinine estimation. *Int. J. Health Sci. (Qassim)* **2021**, *15* (6), 16−22.

(6) Esplin, M. S.; Merrell, K.; Goldenberg, R.; Lai, Y.; Iams, J. D.; Mercer, B.; Spong, C. Y.; Miodovnik, M.; Simhan, H. N.; van Dorsten, P.; et al. Proteomic identification of serum peptides predicting subsequent spontaneous preterm birth. *Am. J. Obst Gynecol* **2011**, *204* (5), 391.e1.

(7) Khambalia, A. Z.; Collins, C. E.; Roberts, C. L.; Morris, J. M.; Powell, K. L.; Tasevski, V.; Nassar, N. High maternal serum ferritin in early pregnancy and risk of spontaneous preterm birth. *Br. J. Nutr.* **2015**, *114* (3), 455−461.

(8) Honest, H.; Lucas, M. B.; Janesh, K. G.; Jos, K.; Khalid, S. K. Accuracy of cervicovaginal fetal fibronectin test in predicting risk of spontaneous preterm birth: systematic review. *BMJ.* **2002**, *325* (7359), 301.

(9) Hsu, T.-Y.; Tsai, K.-W.; Lan, K.-C.; Hung, H.-N.; Lai, Y.-J.; Cheng, H.-H.; Tsai, C.-C.; Li, S.-C. Identifying the potential protein biomarkers of preterm birth in amniotic fluid. *Taiwa J. Obstet Gynecol* **2020**, *59* (3), 366−371.

(10) Gondane, P.; Kumbhakarn, S.; Maity, P.; Kapat, K. Recent Advances and Challenges in the Early Diagnosis and Treatment of Preterm Labor. *Bioengineering (Basel)* **2024**, *11* (2), 161.

(11) Saade, G. R.; Boggess, K. A.; Sullivan, S. A.; Markenson, G. R.; Iams, J. D.; Coonrod, D. V.; Pereira, L. M.; Esplin, M. S.; Cousins, L. M.; Lam, G. K.; et al. Development and validation of a spontaneous preterm delivery predictor in asymptomatic women. *Am. J. Obstet Gynecol* **2016**, *214* (5), 633.e1.

(12) Marić, I.; Stevenson, D. K.; Aghaeepour, N.; Gaudillière, B.; Wong, R. J.; Angst, M. S. Predicting Preterm Birth Using Proteomics. *Clin Perinatol* **2024**, *51* (2), 391−409.

(13) Liu, Y.; Kamran, R.; Han, X.; Wang, M.; Li, Q.; Lai, D.; Naruse, K.; Takahashi, K. Human heart-on-a-chip microphysiological system comprising endothelial cells, fibroblasts, and iPSC-derived cardiomyocytes. *Sci. Rep* **2024**, *14* (1), 18063.

(14) Sontheimer-Phelps, A.; Hassell, B. A.; Ingber, D. E. Modelling cancer in microfluidic human organs-on-chips. *Nat. Rev. Cancer* **2019**, *19* (2), 65−81.

(15) Yrjänäinen, A.; Mesiä, E.; Lampela, E.; Kreutzer, J.; Vihinen, J.; Tornberg, K.; Vuorenpää, H.; Miettinen, S.; Kallio, P.; Mäki, A.-J. Barrier-free, open-top microfluidic chip for generating two distinct, interconnected 3D microvascular networks. *Sci. Rep* **2024**, *14* (1), 22916.

(16) Coluccio, M. L.; Perozziello, G.; Malara, N.; Parrotta, E.; Zhang, P.; Gentile, F.; Limongi, T.; Raj, P. M.; Cuda, G.; Candeloro, P.; et al. Microfluidic platforms for cell cultures and investigations. *Microelectron. Eng.* **2019**, *208*, 14−28.

(17) Dong, X.; Liu, L.; Tu, Y.; Zhang, J.; Miao, G.; Zhang, L.; Ge, S.; Xia, N.; Yu, D.; Qiu, X. Rapid PCR powered by microfluidics: A quick review under the background of COVID-19 pandemic. *Trends Analyt Chem.* **2021**, *143*, 116377.

(18) Men, Y.; Fu, Y.; Chen, Z.; Sims, P. A.; Greenleaf, W. J.; Huang, Y. Digital Polymerase Chain Reaction in an Array of Femtoliter Polydimethylsiloxane Microreactors. *Anal. Chem.* **2012**, *84* (10), 4262−4266.

(19) Yang, S. M.; Lv, S.; Zhang, W.; Cui, Y. Microfluidic Point-of-Care (POC) Devices in Early Diagnosis: A Review of Opportunities and Challenges. *Sensors (Basel)* **2022**, *22* (4), 1620.

(20) Scott, S. M.; Ali, Z. Fabrication Methods for Microfluidic Devices: An Overview. *Micromachines (Basel)* **2021**, *12* (3), 319.

(21) Pradela Filho, L. A.; Paixão, T. R. L. C.; Nordin, G. P.; Woolley, A. T. Leveraging the third dimension in microfluidic devices using 3D printing: no longer just scratching the surface. *Anal Bioanal Chem.* **2024**, *416* (9), 2031−2037.

(22) Su, R.; Wang, F.; McAlpine, M. C. 3D printed microfluidics: advances in strategies, integration, and applications. *Lab Chip* **2023**, *23* (5), 1279−1299.

(23) Sanchez Noriega, J. L.; Chartrand, N. A.; Valdoz, J. C.; Cribbs, C. G.; Jacobs, D. A.; Poulson, D.; Viglione, M. S.; Woolley, A. T.; Van Ry, P. M.; Christensen, K. A.; et al. Spatially and optically tailored 3D printing for highly miniaturized and integrated microfluidics. *Nat. Commun.* **2021**, *12* (1), 5509.

(24) Wang, H.; Enders, A.; Preuss, J.-A.; Bahnemann, J.; Heisterkamp, A.; Torres-Mapa, M. L. 3D printed microfluidic lab-

on-a-chip device for fiber-based dual beam optical manipulation. *Sci. Rep* **2021**, *11* (1), 14584.
(25) Boaks, M.; Roper, C.; Viglione, M.; Hooper, K.; Woolley, A. T.; Christensen, K. A.; Nordin, G. P. Biocompatible high-resolution 3D printed microfluidic devices: integrated cell chemotaxis demonstration. *Micromachines* **2023**, *14*, 1589.
(26) Zhao, M.; Yang, J.; Li, Z.; Zeng, Y.; Tao, C.; Dai, B.; Zhang, D.; Yamaguchi, Y. High-throughput 3D microfluidic chip for generation of concentration gradients and mixture combinations. *Lab Chip* **2024**, *24* (8), 2280−2286.
(27) Shanko, E.-S.; van Buul, O.; Wang, Y.; van de Burgt, Y.; Anderson, P.; den Toonder, J. Magnetic bead mixing in a microfluidic chamber induced by an in-plane rotating magnetic field. *Microfluid Nanofluid* **2022**, *26* (2), 17.
(28) Pedersen-Bjergaard, S.; Rasmussen, K. E. Liquid-phase microextraction with porous hollow fibers, a miniaturized and highly flexible format for liquid−liquid extraction. *J. Chromatogr A* **2008**, *1184* (1), 132−142.
(29) Vergara-Barberán, M.; Carrasco-Correa, E. J.; Lerma-García, M. J.; Simó-Alfonso, E. F.; Herrero-Martínez, J. M. Current trends in affinity-based monoliths in microextraction approaches: A review. *Anal. Chim. Acta* **2019**, *1084*, 1−20.
(30) Almughamsi, H. M.; Howell, M. K.; Parry, S. R.; Esene, J. E.; Nielsen, J. B.; Nordin, G. P.; Woolley, A. T. Immunoaffinity monoliths for multiplexed extraction of preterm birth biomarkers from human blood serum in 3D printed microfluidic devices. *Analyst* **2022**, *147* (4), 734−743.
(31) Campos, C. D. M.; Gamage, S. S. T.; Jackson, J. M.; Witek, M. A.; Park, D. S.; Murphy, M. C.; Godwin, A. K.; Soper, S. A. Microfluidic-based solid phase extraction of cell free DNA. *Lab Chip* **2018**, *18* (22), 3459−3470.
(32) Neumair, J.; D'Ercole, C.; De March, M.; Elsner, M.; Seidel, M.; de Marco, A. Macroporous Epoxy-Based Monoliths Functionalized with Anti-CD63 Nanobodies for Effective Isolation of Extracellular Vesicles in Urine. *Int. J. Mol. Sci.* **2023**, *24* (7), 6131.
(33) Nielsen, J. B.; Holladay, J. D.; Burningham, A. J.; Rapier-Sharman, N.; Ramsey, J. S.; Skaggs, T. B.; Nordin, G. P.; Pickett, B. E.; Woolley, A. T. Monolithic affinity columns in 3D printed microfluidics for chikungunya RNA detection. *Anal Bioanal Chem.* **2023**, *415* (29), 7057−7065.
(34) Chu, W.-Y.; Yang, C.-H.; Viter, R.; Ramanavičius, A.; Luo, S.-C.; Chen, C.-F. Monolith-modified cellulose paper for biochemical sensing applications. *Sens Diagn* **2022**, *1* (5), 994−1002.
(35) Yu, X.; Lai, S.; Wang, L.; Chen, Y.; Lin, X.; Xie, Z. Preparation of aptamer-bound polyamine affinity monolithic column via a facile triazine-bridged strategy and application to on-column specific discrimination of ochratoxin A. *J. Sep Sci.* **2019**, *42* (13), 2272−2279.
(36) Bickham, A. V.; Pang, C.; George, B. Q.; Topham, D. J.; Nielsen, J. B.; Nordin, G. P.; Woolley, A. T. 3D Printed Microfluidic Devices for Solid-Phase Extraction and On-Chip Fluorescent Labeling of Preterm Birth Risk Biomarkers. *Anal. Chem.* **2020**, *92* (18), 12322−12329.
(37) Lyu, Y.; Asoh, T.-A.; Uyama, H. Facile synthesis of a three-dimensional hydroxyapatite monolith for protein adsorption. *J. Mater. Chem. B* **2021**, *9* (47), 9711−9719.
(38) Zhang, X.; Wei, Q.; Meng, X.; Zhao, L.; Liu, Z.; Huang, Y. Boronate Avidity Assisted by Dendrimer-like Polyhedral Oligomeric Silsesquioxanes for a Microfluidic Platform for Selective Enrichment of Ubiquitination and Glycosylation. *Anal. Chem.* **2023**, *95* (2), 1241−1250.
(39) Sousa, A.; Tomaz, C. T.; Sousa, F.; Queiroz, J. A. Successful application of monolithic innovative technology using a carbonyldiimidazole disk to purify supercoiled plasmid DNA suitable for pharmaceutical applications. *J. Chromatogr A* **2011**, *1218* (46), 8333−8343.
(40) Ribeiro, J.; Luís, M. Â.; Rodrigues, B.; Santos, F. M.; Mesquita, J.; Boto, R.; Tomaz, C. T. Cryogels and Monoliths: Promising Tools for Chromatographic Purification of Nucleic Acids. *Gels* **2024**, *10* (3), 198.
(41) Parker, E. K.; Nielsen, A. V.; Beauchamp, M. J.; Almughamsi, H. M.; Nielsen, J. B.; Sonker, M.; Gong, H.; Nordin, G. P.; Woolley, A. T. 3D printed microfluidic devices with immunoaffinity monoliths for extraction of preterm birth biomarkers. *Anal Bioanal Chem.* **2019**, *411* (21), 5405−5413.
(42) Nge, P. N.; Pagaduan, J. V.; Yu, M.; Woolley, A. T. Microfluidic chips with reversed-phase monoliths for solid phase extraction and on-chip labeling. *J. Chromatogr A* **2012**, *1261*, 129−135.
(43) Sahore, V.; Sonker, M.; Nielsen, A. V.; Knob, R.; Kumar, S.; Woolley, A. T. Automated microfluidic devices integrating solid-phase extraction, fluorescent labeling, and microchip electrophoresis for preterm birth biomarker analysis. *Anal Bioanal Chem.* **2018**, *410* (3), 933−941.
(44) Beauchamp, M. J.; Nielsen, A. V.; Gong, H.; Nordin, G. P.; Woolley, A. T. 3D Printed Microfluidic Devices for Microchip Electrophoresis of Preterm Birth Biomarkers. *Anal. Chem.* **2019**, *91* (11), 7418−7425.
(45) Esene, J. E.; Burningham, A. J.; Tahir, A.; Nordin, G. P.; Woolley, A. T. 3D printed microfluidic devices for integrated solid-phase extraction and microchip electrophoresis of preterm birth biomarkers. *Anal. Chim. Acta* **2024**, *1296*, 342338.
(46) Esene, J. E.; Nasman, P. R.; Miner, D. S.; Nordin, G. P.; Woolley, A. T. High-performance microchip electrophoresis separations of preterm birth biomarkers using 3D printed microfluidic devices. *J. Chromatogr A* **2023**, *1706*, 464242.
(47) Bilatto, S. E. R.; Adly, N. Y.; Correa, D. S.; Wolfrum, B.; Offenhäusser, A.; Yakushenko, A. Printed microfluidic filter for heparinized blood. *Biomicrofluidics* **2017**, *11* (3), 034101.
(48) Deiana, G.; Smith, S. 3D Printed Devices for the Separation of Blood Plasma from Capillary Samples. *Micromachines* **2024**, *15* (3), 359.
(49) Garcia-Rey, S.; Nielsen, J. B.; Nordin, G. P.; Woolley, A. T.; Basabe-Desmonts, L.; Benito-Lopez, F. High-resolution 3D printing fabrication of a microfluidic platform for blood plasma separation. *Polymers* **2022**, *14* (13), 2537.
(50) Gilquin, B.; Cubizolles, M.; Den Dulk, R.; Revol-Cavalier, F.; Alessio, M.; Goujon, C.-E.; Echampard, C.; Arrizabalaga, G.; Adrait, A.; Louwagie, M.; et al. PepS: An Innovative Microfluidic Device for Bedside Whole Blood Processing before Plasma Proteomics Analyses. *Anal. Chem.* **2021**, *93* (2), 683−690.
(51) Tatar, N.; Akgönüllü, S.; Yavuz, H.; Denizli, A. Cibacron Blue F3GA ligand dye-based magnetic silica particles for the albumin purification. *Turk J. Chem.* **2023**, *47* (5), 1125−1137.
(52) Lee, P. Y.; Osman, J.; Low, T. Y.; Jamal, R. Plasma/Serum Proteomics: Depletion Strategies for Reducing High-Abundance Proteins for Biomarker Discovery. *Bioanalysis* **2019**, *11* (19), 1799−1812.

https://doi.org/10.1021/prechem.4c00092
Precis. Chem. 2025, 3, 261−271